



Article

# An Efficient Indoor Wi-Fi Positioning Method Using Virtual Location of AP

Fan Xu <sup>1</sup> , Xuke Hu <sup>2,3</sup> , Shuaiwei Luo <sup>1,4,\*</sup> and Jianga Shang <sup>1</sup>

<sup>1</sup> School of Geography and Information Engineering, China University of Geosciences, Wuhan 430078, China; xufan12321@cug.edu.cn (F.X.); jgshang@cug.edu.cn (J.S.)

<sup>2</sup> Institute of Data Science, DLR, 07745 Jena, Germany; xuke.hu@dlr.de

<sup>3</sup> GIScience Research Group, Institute of Geography, Heidelberg University, 69117 Heidelberg, Germany

<sup>4</sup> College of Tourism and Planning, Pingdingshan University, Pingdingshan 467000, China

\* Correspondence: 2834@pdsu.edu.cn

Received: 19 February 2020; Accepted: 16 April 2020; Published: 19 April 2020



**Abstract:** Wi-Fi fingerprinting has been widely used for indoor localization because of its good cost-effectiveness. However, it suffers from relatively low localization accuracy and robustness owing to the signal fluctuations. Virtual Access Points (VAP) can effectively reduce the impact of signal fluctuation problem in Wi-Fi fingerprinting. Current techniques normally use the Log-Normal Shadowing Model to estimate the virtual location of the access point. This would lead to inaccurate location estimation due to the signal attenuation factor in the model, which is difficult to be determined. To overcome this challenge, in this study, we propose a novel approach to calculating the virtual location of the access points by using the Apollonius Circle theory, specifically the distance ratio, which can eliminate the attenuation parameter term in the original model. This is based on the assumption that neighboring locations share the same attenuation parameter corresponding to the signal attenuation caused by obstacles. We evaluated the proposed method in a laboratory building with three different kinds of scenes and 1194 test points in total. The experimental results show that the proposed approach can improve the accuracy and robustness of the Wi-Fi fingerprinting techniques and achieve state-of-art performance.

**Keywords:** indoor positioning; Wi-Fi fingerprinting; virtual AP; Apollonius circle

## 1. Introduction

To date, various indoor positioning technologies have been proposed to meet the increasing requirement of indoor ubiquitous location services [1], such as Pedestrian Dead Reckoning (PDR) [2–4], acoustic-based [5,6], visual-based [7,8], radio frequency-based [9,10], and magnetic field-based techniques [11,12]. Due to the popularity of Wi-Fi infrastructure and Wi-Fi-embedded mobile equipment, Wi-Fi-based positioning techniques have become increasingly popular. For example, the Channel State Information (CSI) [13] and Received Signal Strength Indication (RSSI) can be extracted from Wi-Fi Access Points (APs), which showed good potential in indoor localization. However, CSI data cannot be collected from current smartphones since it is the signal at the physical level of Wi-Fi networks. Therefore, this study focuses on RSSI-based indoor localization techniques, which are readily accessed from Android smartphones. Typically, Wi-Fi positioning techniques can be coarsely divided into two categories: fingerprinting-based [14–19] and ranging-based [20–33]. The former can be implemented with machine learning methods [10,34–37] and machine learning-free methods [10,38]. This study investigates the Weighted K Nearest Neighboring (WKNN), which is a representative approach of the machine learning-free fingerprinting techniques since it can achieve an acceptable localization accuracy with a low computational complexity. Ranging-based techniques typically use the RSSI to calculate

the distances between the Mobile Node (MN) and Wi-Fi APs, then obtain the location of the MN by geometric methods. Nowadays, fingerprinting techniques gain much more attention than ranging-based ones. This is attributable to two reasons. The first is that the ranging techniques require the physical location and transmission power parameters of APs, which however are difficult to be determined. For instance, the locations of many APs, especially in smart space, are changeable. The second is the signal attenuation, which happens frequently in the indoor complex environment. This would lead to inaccurate ranging based on RSSI.

Normally, fingerprinting approaches are more robust than ranging-based methods in complex environments. The pure WKNN, which is a representative fingerprinting approach, needs to select the closest reference points (RPs) by the similarity of RSSI between RPs and test points. This is, however, susceptible to the fluctuation of signal caused by obstacles. To overcome this challenge, landmarks, such as the stairs, elevators, and corners, where distinct sensor reading can be detected, are normally used to calibrate the estimated location [17,18,39]. However, it is very common that no landmarks exist in certain indoor environments. Faced with this challenge, some researchers have proposed using virtual AP methods to aid WKNN by introducing nonlinear constraints [40]. The Log-Normal Shadowing Model is normally used to estimate the virtual location of the APs [40–42], which is inaccurate due to the difficulty of determining the signal attenuation factor in the model.

To reduce the location estimation error of the virtual APs, in this study, we propose a novel signal strength ratio-based method. In the offline phase, we first use the location and signal ratio of RPs to construct Apollonius circles [43]. During this procedure, the transmission power parameter, which is used in the Log-Normal Shadowing Model to calculate the distance, can be eliminated. Furthermore, the location estimation error caused by the unknown attenuation factor can be also eliminated. Then, the virtual location of the AP is obtained by calculating the intersection point of circles with least squares. In the online phase, the initial area where the MN is currently located is first determined with the RSSI vector. Then, the location of the MN is refined based on the virtual locations of APs calculated by RPs in the initial area. Specifically, the precise position of the MN is determined by the least squares and the Apollonius circles formed by the virtual locations of the APs. In general, our main contribution is proposing a novel approach to estimate the virtual location of APs, which is integrated with the Wi-Fi fingerprinting technique. This can improve the robustness and accuracy of Wi-Fi fingerprinting.

The remainder of the paper is organized as follows: Section 2 reviews related work and current technology. Section 3 presents the basic idea and theory of our method. Section 4 introduces the workflow and the details of the proposed method. We evaluate the performance of the proposed method in Section 5 and compare it to the state-of-the-art. Conclusions and future work are discussed in Section 6.

## 2. Related Work

Our proposed approach involves fingerprinting, signal propagation model-based ranging, and virtual AP techniques. Therefore, in this section, we conduct the literature overview of the fingerprinting and ranging-based approaches and how previous studies used virtual APs for localization.

### 2.1. Fingerprint-Based Methods

Typically, fingerprinting localization can be divided into two categories: machine learning [10,34–37] and machine learning-free [40,44–53]. Both techniques consist of two stages: offline training and online tagging. The core of the fingerprinting is associating Wi-Fi signal vectors with the spatial location of an indoor environment. The difference lies in the requirement of learning a model or not:

- Machine learning methods. During the offline stage, a model is trained to associate signal vectors with spatial locations. During the online stage, the model is used to predict the location of a mobile target given the signal vector collected at the current location from surrounding APs. For instance, Wang et al. [10] proposed a deep-learning-based indoor fingerprinting system for indoor positioning called DeepFi, using a greedy learning algorithm to train the weights layer-by-layer to reduce

complexity. Dai et al. [34] proposed an MLNN method, which integrates the RSSI transforming, the raw data denoising, and the unknown node locating into a deep architecture, moreover, avoiding using RSSI map in the online stage. To reduce the required computational cost and time, Extreme Learning Machine (ELM) is utilized in the work of Khatab et al. [35]. It also uses the autoencoder instead of random weight generation that leads to discriminative feature extraction and the improvement of localization performance. Among these methods, most of them use machine learning to find out the inner pattern behind MN data to match the RP data. However, outer constraints, such as landmarks, are still irreplaceable when facing the attenuation caused by obstacles.

- Machine learning-free methods. The representative method is WKNN [44]. It uses different similarity metrics to measure the distance between MNs and the selected RPs and then assigns a higher weight to the closer RP [40,45–47,49–54]. Feng et al. [45] reckon that the localization problem can be modeled as a sparse problem. Therefore, they use the theory of compressive sensing to recover sparse signals from a small number of noisy measurements. This can address the geographical dispersion of selected RPs caused by the inconsistency between signal space and physical space. He et al. [47] proposed partitioning the coverage area of each AP. Then, through convex optimization, the user is localized based on the cluster and the junction of the sectors it is within. Apart from these, room-level localization also gains much attention. For instance, Jiang et al. [49] used a zone-based clustering algorithm to identify an in-room occupancy hotspot. Then, a motion-based clustering algorithm is used to identify interzone correlation, thereby distinguishing different rooms.

## 2.2. Ranging-Based Methods

Ranging-based methods are typically used in sensor networks [30], using the distance calculated by Time of Arrival (TOA), Time Different of Arrival (TDOA), Angle-of-Arrival (AOA), or RSSI to obtain the locations of mobile targets, which can significantly reduce the dependency on fingerprints. In this paper, we focus on the RSSI based ranging approach to obtain the location of virtual APs. An RSSI based ranging approach can be further divided into two categories:

- Distance-based approaches. It calculates the distances between the location known infrastructures (e.g., AP) and the MN. Then, the geometric methods such as triangulation are used to estimate the exact locations of MNs. However, the frequently happened signal attenuation would cause the inaccuracy of location calculation. To address this issue, the method proposed by Dag et al. [23] used the least squares algorithm to improve the reliability of RSSI measurements. Similarly, the least squares algorithm is also used in the work of Coluccia et al. [27] to achieve a higher positioning accuracy. Apart from least squares approaches, many other methods have also been proposed to deal with the signal attenuation issue. For instance, Jung et al. [24] used particle filters to infer the possible location of the MN and the possible signal propagation path. Then, the inferred path is used to reduce the error caused by NLOS (Non-Line-of-Sight) distance. Chuang et al. [25] adopted the Particle Swarm Optimization (PSO) algorithm to improve the localization accuracy and the DV-distance approach to further boost the success ratios of localization. Chan et al. [26] proposed a geometric method to locate the MN, which requires only a few APs. Most of the distance-based approaches use the Log-Normal Shadowing Model to estimate the distance between APs and mobile targets. However, the attenuation is a vital parameter which is difficult to be obtained. In the aforementioned methods, this parameter is normally ignored, which reduces the accuracy of the ranging approach.
- Area-based methods. In these methods, people use a vague distance relationship, such as far from or close to the specific AP, calculated by RSSI to locate the rough area of the MN. Then, the centroid of the area is determined, which is regarded as the location estimation of the MN. However, the shape of the area varies. For instance, He et al. [32] used the change of RSSI from moving MNs to determine a triangle area constructed by APs. The MN is thus located in this triangle area.

Sheu et al. [33] proposed an improved grid-scan algorithm to determine the estimated locations in a circle area. The circle area is constructed by the coverage of AP signals. Liu et al. [28] proposed using the RSSI differences received from distinct APs to construct a ring area where the mobile target is possibly located. Elbakly et al. [30] used the Voronoi diagram of APs to estimate the possible area of the MNs. The area-based approaches leverage the signal strength to determine a rough area, which is more robust than calculating physical distance with the signal strength. This can effectively reduce the impact of signal attenuation, but it can only provide area-level positioning accuracy, which can not meet the requirement of many Location Based Services (LBS) applications.

### 2.3. Virtual AP-Based Methods

The virtual AP is a new technique used to enhance the fingerprinting, which can be divided into two categories. The first uses interpolation methods to increase the density of APs [55,56]. It is applied in the scenes where APs are sparsely distributed to improve the location estimation accuracy of fingerprinting. For instance, Labinghisa et al. [55] used RSSI from multiple APs to generate virtual APs and new signal fingerprints through a linear regression statistical model. Then, the Kalman filter (KF) and particle filter (PF) were used to reduce the noise of the RSSI collected in the online stage. The second uses positioning techniques to obtain the virtual location of APs [40–42]. Our proposed method belongs to the second type. Different from the first type, the second method does not increase the density of virtual APs but estimates the virtual location of existing APs instead. In this situation, the virtual AP-based approaches are used in the scenes where the location of APs cannot be easily acquired. For instance, in the work of Mo et al. [41], Cuckoo search via Lévy flight is executed to obtain the first estimation of the AP parameters, and then the estimated AP parameters are further refined with the Quasi-Newton algorithm. Then, in the online phase, they use signal strength differences (SSD) instead of RSSI to calculate the Euclidean distance between users and RPs. In the work of Xue et al. [40], the virtual AP is obtained by the Log-Normal Shadowing Model. They use the calculated distance and Nelder–Mead simplex algorithm to estimate the virtual location of APs. Then, the virtual locations of APs are only used to cluster the nearest reference points in the online stage. Specifically, the physical distance rather than signal distance is used to assign weights for the location estimation. Furthermore, virtual AP methods can also be used in multi-floor situations. For instance, Liu et al. [42] used a similarity metric to determine the accurate floor of the mobile target, then the location of virtual APs between different floors is estimated by a weighted screening (WS) method. Finally, these virtual APs are used to calculate the precise position of mobile targets by trilateration. Currently, how to accurately estimate the virtual location of APs is still a challenge. To solve this problem, we propose a signal strength ratio-based method to estimate the virtual locations of the APs.

## 3. Signal Strength Ratio-Based Location Solver

In this section, we introduce our theories and assumptions and then discuss how the algorithm works without directly calculating the physical distance.

### 3.1. Signal Strength Ratio

Based on the assumption that the signal received from neighboring locations would experience the same signal attenuation, we use the signal strength ratio rather than the absolute physical distance to estimate the virtual location of APs. In the original signal attenuation model formalized as Equation (1), the attenuation item, which refers to the attenuation factor caused by obstacles is difficult to determine:

$$RSSI_k(d_{ki}) = RSSI_k(d_{k0}) - 10\eta \log_{10}\left(\frac{d_{ki}}{d_{k0}}\right) - OAF \quad (1)$$

where  $RSSI_k(d_{ki})$  is the received signal strength from the location that is far away from  $AP_k$  at a distance  $d_{ki}$ .  $RSSI_k(d_{k0})$  is the received signal strength from the location that is far away from  $AP_k$  at a

distance  $d_{k0}$ .  $\eta$  is the path loss exponent, generally ranging from 1.6 to 3.0 according to the complexity of the scene. The Obstacle Attenuation Factor (OAF) denotes the signal attenuation caused by obstacles. Typically, we set  $d_{k0}$  to 1 m. Then,  $d_{ki}$  can be calculated by Equation (2):

$$d_{ki} = 10^{\left(\frac{RSSI_k(d_{k0}) - RSSI_k(d_{ki}) - OAF}{10\eta}\right)} \quad (2)$$

Different from other algorithms, the proposed method does not directly use the distance calculated by the Log-Normal Shadowing Model to estimate the locations of MNs. Since the  $OAF$  and  $RSSI_k(d_{k0})$  cannot be easily obtained, we use the ratio of  $d_{ki}$  and  $d_{kj}$ , which are the distances from location  $i$  and  $j$  to  $AP_k$ , respectively. The ratio can be calculated by Equation (3):

$$R = \frac{d_{ki}}{d_{kj}} = 10^{\left(\frac{RSSI_k(d_{k0}) - RSSI_k(d_{ki}) - OAF_i - RSSI_k(d_{k0}) + RSSI_k(d_{kj}) + OAF_j}{10\eta}\right)} \quad (3)$$

The location  $i$  and  $j$  we choose are physically close. Thus, the path the signal propagates from  $AP_k$  to location  $i$  is similar to the path from  $AP_k$  to location  $j$ . This means they have approximating signal attenuation. Therefore,  $OAF_i$  and  $OAF_j$  can be assumed equal.  $RSSI_k(d_{k0})$  from location  $i$  equals that from location  $j$ . Thus, Equation (3) can be rewritten as Equation (4):

$$R = \frac{d_{ki}}{d_{kj}} = 10^{\left(\frac{RSSI_k(d_{kj}) - RSSI_k(d_{ki})}{10\eta}\right)} \quad (4)$$

Now, we can calculate the ratio without the need of knowing the value of  $OAF$  and  $RSSI_k(d_{k0})$ . This means that the proposed method requires less information from the APs for the location estimation. Most importantly, it avoids the calculation of  $OAF$ , which is normally difficult to be accurately determined and thus reduces the location estimation accuracy.

### 3.2. Apollonius Circle

In our proposed model, only the distance ratio is supposed to be calculated without the need for calculating the absolute distance by using the traditional Log-Normal Shadowing Model. Specifically, only  $RSSI$  and  $\eta$  are required. Given the distance ratio, the Apollonius circle is then used to calculate the virtual location of APs. The ratio  $R$  can be calculated according to formulas (5)–(7).

$$d_{ki} = \sqrt{(x_i - x_k)^2 + (y_i - y_k)^2} \quad (5)$$

$$d_{kj} = \sqrt{(x_j - x_k)^2 + (y_j - y_k)^2} \quad (6)$$

$$R = \frac{d_{ki}}{d_{kj}} = \frac{\sqrt{(x_i - x_k)^2 + (y_i - y_k)^2}}{\sqrt{(x_j - x_k)^2 + (y_j - y_k)^2}} \quad (7)$$

where  $(x_i, y_i)$  and  $(x_j, y_j)$  are the 2-dimension coordinate of location  $i$  and  $j$ , respectively, and  $(x_k, y_k)$  is the coordinate of  $AP_k$ . As shown in Figure 1, the proposed method only calculates the distance ratio, and the absolute distance between the reference point and AP remains unknown. Then, the virtual location of APs can be calculated by Equation (7), which can be rewritten as Equation (8):

$$x_k^2 + y_k^2 + \frac{2x_j R^2 - 2x_i}{1 - R^2} x_k + \frac{2y_j R^2 - 2y_i}{1 - R^2} y_k + \frac{x_i^2 + y_i^2 - x_j^2 R^2 - y_j^2 R^2}{1 - R^2} = 0 \quad (8)$$

Then, we set the  $\frac{2x_j R^2 - 2x_i}{1 - R^2}$  as  $D$ ,  $\frac{2y_j R^2 - 2y_i}{1 - R^2}$  as  $E$ , and  $\frac{x_i^2 + y_i^2 - x_j^2 R^2 - y_j^2 R^2}{1 - R^2}$  as  $F$ . The equation is rewritten as Equation (9):

$$x_k^2 + y_k^2 + Dx_k + Ey_k + F = 0 \quad (9)$$

According to the Apollonius theory [43], a circle can be defined as the set of points in a plane with a specified distance ratio to two fixed points. As we can see, Equation (9) is the general form of the equation of circles. When  $D^2 + E^2 - 4F > 0$ , the possible location of APs is then on a circle. In addition, when  $R = 1$ , the possible location of APs is obviously on the vertical bisector of location  $i$  and  $j$ .

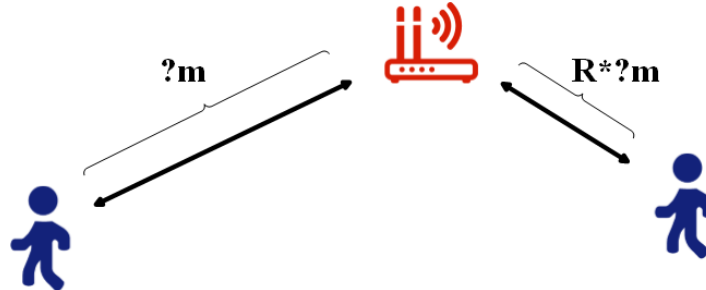


Figure 1. Virtual location estimation of APs without the absolute distance.

### 3.3. Virtual AP

According to Equation (3), the parameter  $OAF$  can be eliminated when the locations of reference points are close enough because the received signals from these locations propagate through a similar path. As shown in Figure 2a, in an ideal environment, the geometric methods, such as triangulation, can be used to calculate the location of APs. The calculated distance approximates the real distance. In Figure 2b, the received signals are significantly weaker than that in an ideal environment due to the attenuation caused by walls. This means that the calculated distance will be larger than the real distance. In this case, the geometric methods thus cannot be used to calculate the position of the AP. However, due to the signals received by close reference points have passed through the same obstacle, the attenuation of signals is thus similar. As shown in Figure 2c, the decreased signals can be used to estimate the location of APs, which is named the virtual location of APs. Then, we can use the virtual location of APs to estimate the location of the close MN.

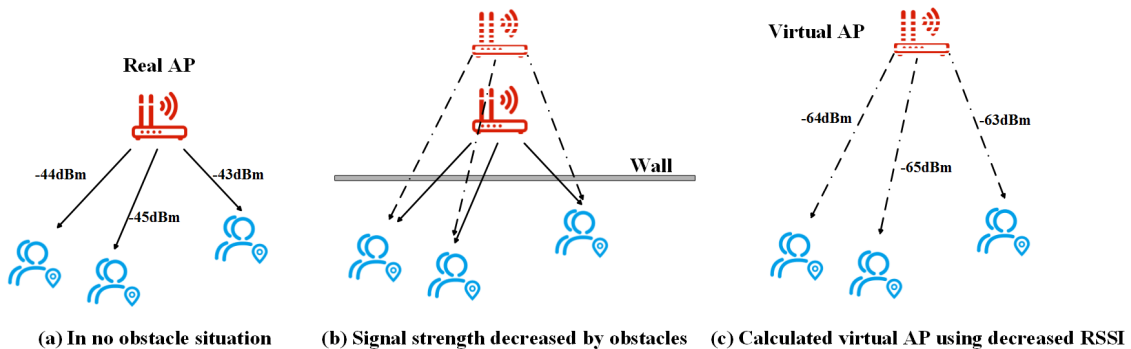


Figure 2. Virtual location of APs under attenuated signals.

## 4. Proposed Method

This proposed approach uses fingerprint-based positioning techniques. Thus, the fingerprint database should be first constructed during the offline stage. As shown in Figure 3, our proposed method can be divided into two phases: the offline phase and the online phase. During the offline stage, the floor plan is first divided into multiple smaller regions according to the spatial structure to reduce the computational complexity. Then, the virtual location of APs in each divided region is estimated. In the online phase, the initial area the MN locates is first determined. Then, the location of the MN is refined by using the virtual location of APs with the geometric method.

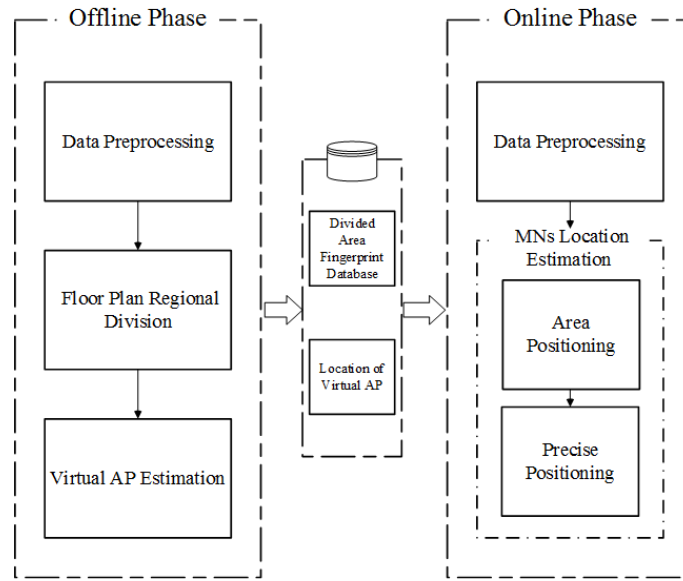


Figure 3. Workflow of the proposed method.

#### 4.1. Data Preprocessing

To mitigate the fluctuation of the received signal, previous studies have found that using maximum RSSI produces better positioning accuracy than using mean RSSI in general [57]. Therefore, in the data preprocessing module of the proposed method, we first rank the received RSSI at each location in descending order. Then, the ordered data are processed with Equation (10):

$$\overline{RSSI}_i^k = \frac{RSSI_{i1}^k + RSSI_{i2}^k + RSSI_{i3}^k}{3} \quad (10)$$

where  $RSSI_{i1}^k$  is the maximum RSSI value at location  $i$  of  $k_{th}$  AP, and  $RSSI_{i2}^k$  and  $RSSI_{i3}^k$  are the second and third maximum RSSI value at location  $i$  of  $k_{th}$  AP, respectively.

#### 4.2. Region Division

Based on the theory of virtual AP, the proposed method works when the reference points are close to each other. This means that, if we want to locate the position of the MN, we have to select the adjacent reference points of the MN to calculate the virtual AP firstly. To reduce the calculation in the online stage and ensure that the adjacent RPs are located in a similar environment, the proposed method uses the floor plan of the test environment to divide the reference points into different physical regions. The RPs in the same region share the same virtual AP positions. In this study, the regions are divided based on two rules. The first is that the interval between two RPs is no more than 10 m and no more than 10 RPs are located in one region. The second is that the RPs in the same region should be in the same segment of a corridor.

#### 4.3. Virtual AP Estimation

In each region, the virtual APs will be calculated independently. Based on Equation (8), a circle can be obtained based on two RPs. Thus, theoretically, at least three reference points are needed to obtain three circles. Then, the virtual location of APs can be estimated by calculating the intersection point of the three circles. However, as shown in Figure 4, due to the measurement error of RSSI, it is nearly impossible to obtain a unique intersection point from three or more than three circles. Therefore, in this study, we use the least squares algorithm to estimate the coordinates of the point with the smallest sum of squares of the distances to all Apollonius circles, based on which the position of the MN can be obtained. This process can be described as Equation (11):

$$(\hat{x}, \hat{y}) = \arg \min_{x,y} \sum_{i=1}^n \bar{w}_i \left( \sqrt{\left(x + \frac{D_i}{2}\right)^2 + \left(y + \frac{E_i}{2}\right)^2} - \frac{1}{2} \sqrt{D_i^2 + E_i^2 - 4F_i} \right)^2 \quad (11)$$

Then, we set the  $-\frac{D_i}{2}$  as  $x_i$ ,  $-\frac{E_i}{2}$  as  $y_i$ ,  $\frac{1}{2} \sqrt{D_i^2 + E_i^2 - 4F_i}$  as  $r_i$ . The equation is thus rewritten as Equation (12):

$$(\hat{x}, \hat{y}) = \arg \min_{x,y} \sum_{i=1}^n \bar{w}_i \left( \sqrt{(x - x_i)^2 + (y - y_i)^2} - r_i \right)^2 \quad (12)$$

where  $(x_i, y_i)$  is the center of the circle calculated by Equation (9),  $r_i$  is the radius of the circle, and  $\bar{w}_i$  is the weight of each circle. Due to the error of the measured signal strength, we assign a lower weight to the RSSI that has propagated a long distance. Then,  $\bar{w}_i$  can be calculated by Equations (13) and (14):

$$w_i = \log_{10} R_i \quad (13)$$

$$\bar{w}_i = \frac{w_i}{\sum_{i=1}^n w_i} \quad (14)$$

where  $R_i$  is calculated by Equation (4).

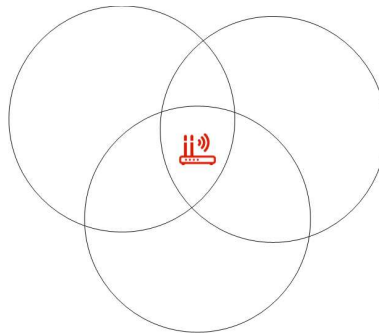


Figure 4. Virtual AP estimation.

#### 4.4. Mobile Node Location Estimation

The online location estimation phase consists of two steps. The first is to determine in which region the MN is located by calculating the signal distance between signal vectors collected at the current location to all the RPs in the database. The region which the closest RP belongs to is treated as the current region of the MN. The signal distance is calculated by Equation (15):

$$S_i = \sqrt{\sum_{k=1}^n (RSSI^k - RSSI_i^k)^2} \quad (15)$$

where  $RSSI^k$  is the RSSI the MN receives from  $k_{th}$  AP, and  $RSSI_i^k$  is the signal received from  $k_{th}$  AP at reference location  $i$ . Then,  $RSSI_k(d_{k0})$  is calculated by Equation (16):

$$RSSI_k(d_{k0}) = RSSI_k(d_{ki}) + 10\eta \log_{10} \left( \frac{d_{ki}}{d_{k0}} \right) + OAF \quad (16)$$

where  $d_{k0}$  is usually set as 1 meter and the  $d_{ki}$  is calculated by the virtual location of APs and RPs. Then, Equation (3) can be rewritten as Equation (17):

$$R = \frac{d_{ku}}{d_{mu}} = 10^{\left( \frac{RSSI_m(d_{mu}) - RSSI_k(d_{ku}) + RSSI_k(1) - RSSI_m(1)}{10\eta} \right)} \quad (17)$$

where  $RSSI_m(d_{mu})$  and  $RSSI_k(d_{ku})$  are the  $m_{th}$  and  $k_{th}$  AP signals received from the MN, respectively. Then, we can use the same method that has been used in the virtual AP estimation phase to estimate the precise location of the MN.



## 5. Evaluation

We choose the fourth floor of the engineering laboratory building of the China University of Geosciences as the test site. It is 85 m  $\times$  52 m, containing corridors, offices, labs, and elevators. The offline and online experimental data are collected through Google's Nexus phone. The interval of the reference points is one meter, which is shown in Figure 5. The constructed fingerprint database includes the coordinates of the reference points, which were measured by an electronic total station and RSSI from surrounding APs. The signal sampling rate of the phone is 1 Hz and, at each reference point, we conducted collections 10 times. In total, 332 RPs were collected. Thirty-three experimental paths were planned in the building with the length ranging from 34 m to 141 m. The total length of the paths is about 1600 m. Finally, 1194 test points were collected by pedestrians walking along the experimental path at a constant speed. To obtain the true locations of test points, we first selected each inflection point on the path as the mark point. The true locations of the mark points were measured with the electronic total station. During the segment of two mark points, testers walked at a constant speed. Thus, the true location of each test point can be obtained through interpolation between two mark points. The spatial distribution of the test points is shown in Figure 6.

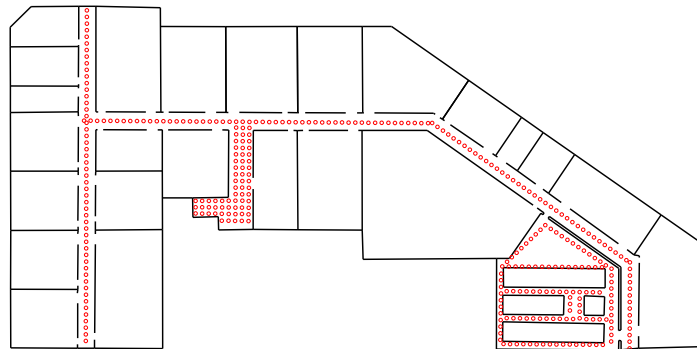


Figure 5. Reference points in the test site.

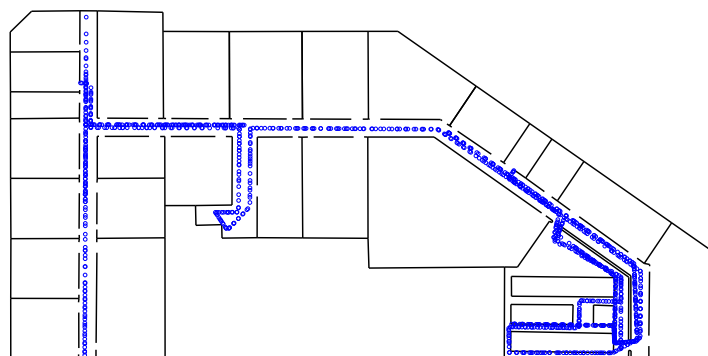


Figure 6. Test points in the test site.

To evaluate the performance of the proposed approach, the proposed method is compared with the three representative Wi-Fi-based approaches. They are a classical fingerprinting method named RADAR [58], a novel ranging-based method named Iterative Positioning Algorithm (IPA) [59], and a virtual AP-based method named PD-WKNN [40].

### 5.1. Impact of Test Scenes on Positioning Accuracy

Different indoor environments contain different spatial structures and sources of interference, which would affect the performance of positioning algorithms. To comprehensively evaluate the proposed approach, the testbed is further divided into three different scenes, as shown in Figure 7.

They are the corridor scene, obstacle-free office scene, and complex office scene. The chosen corridor is a classic corridor environment that has limited walking space and no obstacles. In this area, there are 682 test points. The obstacle-free office scene is a typical office but without any obstacles, such as desks or bookcases. In this region, there are 105 test points. The complex office scene is more spacious than the second scene with numerous tables and pillars. Its area is 302 m<sup>2</sup>. There are 407 test points in this scene. The environmental parameter  $\eta$  is set as 2.4.

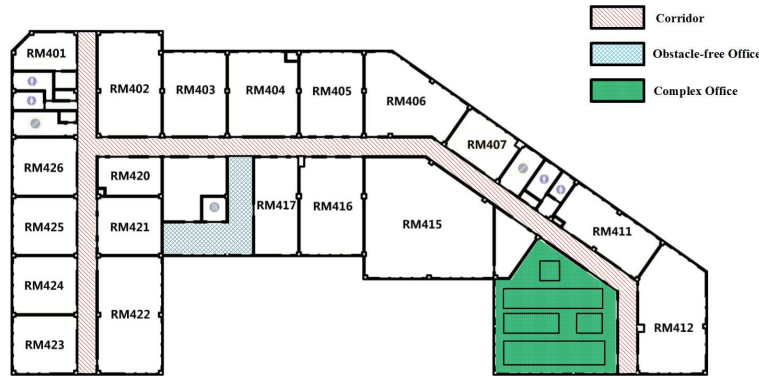


Figure 7. Three different areas of the test site.

As shown in Figure 8, the proposed method shows good performance in the three different scenes. In the complex office region with many obstacles that can lead to attenuation, PD-WKNN achieved the worst performance, limiting 70% of location error under 6.5 m. By contrast, since the attenuation parameters in the propagation model have been eliminated, the proposed method is more robust in this environment, limiting 70% of location error under 3.3 m. In the corridor region, the proposed method still achieved the best performance among the four methods, limiting 70% of location error under 3.3 m. In the obstacle-free office region, all four methods achieved good localization accuracy. In 70% of the cases, the location errors of the four methods are under 3.1 m. RADAR achieved the highest accuracy in this scene, which is followed by our proposed method. In the obstacle-free region, which is an ideal signal propagation environment, the biggest factor affecting the localization accuracy is not the signal attenuation caused by obstacles but the unstable RSSI caused by the signal fluctuation. In this case, RADAR, which simply compares the signal similarity of the online signal vector and the offline reference points, can thus achieve the best performance. The remaining methods, including the proposed method, use the signal propagation model to deal with the attenuation caused by obstacles, introducing extra errors. Therefore, although the accuracy of these methods has been improved in this simple environment compared to that of another two complex environments, the improvement is not as obvious as RADAR.

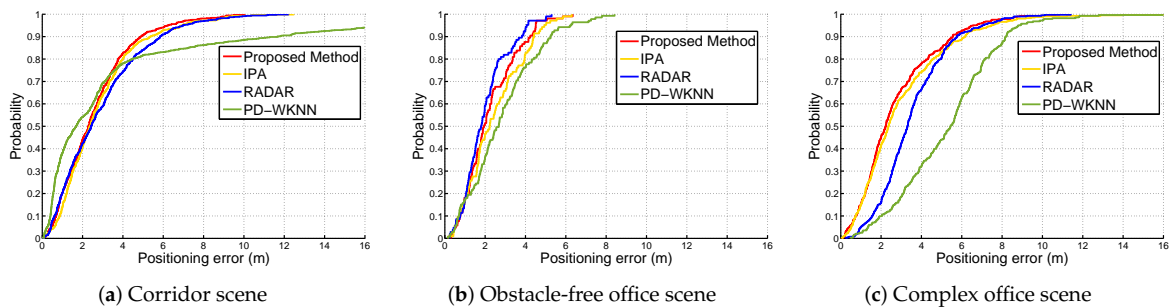


Figure 8. Performance comparison of the proposed method against ranging, fingerprinting, and virtual AP methods in three typical scenes.

Among the compared methods, RADAR has the lowest computational complexity, which is followed by the proposed method and PD-WKNN with medium computational complexity, while IPA

has the highest computational complexity. As shown in Table 1, in the simplest indoor scenario (i.e., the obstacle-free office), RADAR achieves the highest accuracy with the lowest computational complexity. Thus, it is the best choice for localization in a simple indoor scenario. However, as the increase in the complexity of the scene, RADAR shows a decrease in the localization accuracy since it cannot handle the increasing signal attenuation issue. In the complex office scene, the mean error of the proposed method is 23% lower than that of RADAR. For the entire test site, the proposed method achieves the best localization result, which is followed by IPA. Overall, the proposed method achieves the best localization result with an acceptable computational complexity, especially in complex indoor scenes.

**Table 1.** Mean error of the proposed method against fingerprinting, ranging, and virtual AP methods in three typical scenes.

	Proposed Method	IPA	RADAR	PD-WKNN
Corridor scene	2.60 m	2.80 m	2.89 m	3.62 m
Obstacle-free office scene	2.24 m	2.45 m	1.99 m	2.86 m
Complex office scene	2.75 m	3.00 m	3.56 m	5.28 m
Total	2.62 m	2.84 m	3.04 m	4.12 m

## 5.2. Impact of Environmental Parameter on Positioning Accuracy

To analyze the impact of the environmental parameter  $\eta$  of the Log-Normal Shadowing Model on the localization performance, this parameter is set to different values in different indoor scenes. The value of  $\eta$  generally ranges from 1.6 to 3.0. In the previous experiment, we simply set it as the intermediate value of 2.4. In this experiment, we set  $\eta$  as 1.6, 2.0, 2.4, 2.8, and 3.2, respectively.

As shown in Table 2, with the increase of  $\eta$ , the localization accuracy shows a subtle but stable downward trend. Parameter  $\eta$  reflects the complexity of the indoor environment. The more complex the indoor environment, the larger  $\eta$  should be. In a simple environment,  $\eta$  is generally set to 1.6. The model adjusts the effect of different spatial layout on the calculated distance through parameter  $\eta$ . However, the virtual AP-based method assumes that the signal propagates in an obstacle-free environment and comes from the calculated virtual location. The distance from the virtual location to the MN is usually larger than the true distance from the AP to the MN. Based on the assumption that the signals received by neighboring MNs from the same AP have undergone similar attenuation, the virtual AP method makes use of the distance error caused by similar signal attenuation. Therefore, a lower parameter  $\eta$  setting is more in line with the hypothetical environment of the proposed method. In the classic corridor scene, the best  $\eta$  value is 1.6 or lower for the proposed method.

**Table 2.** Impact of different environmental parameters on positioning accuracy in the corridor scene.

	Mean Error (m)	Median Error (m)	70% Error (m)
$\eta = 1.6$	2.59	2.27	3.21
$\eta = 2.0$	2.60	2.27	3.19
$\eta = 2.4$	2.60	2.29	3.22
$\eta = 2.8$	2.61	2.30	3.25
$\eta = 3.2$	2.61	2.30	3.25

From Table 3, we can observe that, with the increase of  $\eta$ , the 70% error also slightly increases except when  $\eta = 3.2$ . The mean error also shows a slight but steady upward trend as the increase of  $\eta$ . This proves that, in general, when  $\eta$  is set to a lower value, the performance of the proposed method is better. However, we also note that the median error does not present the same trend. Due to the small variation of the error and the unstable trend, we can not determine the cause of this phenomenon. Based on the experimental results, we can only conclude that, for the proposed method, the optimal  $\eta$  value ranges from 1.6 to 2.0 in simple office environments.

**Table 3.** Impact of different environmental parameters on positioning accuracy in the obstacle-free office scene.

	Mean Error (m)	Median Error (m)	70% Error (m)
$\eta = 1.6$	2.22	1.98	2.77
$\eta = 2.0$	2.21	1.95	2.79
$\eta = 2.4$	2.24	1.95	2.82
$\eta = 2.8$	2.25	1.96	2.87
$\eta = 3.2$	2.28	1.93	2.80

From Table 4, we can see that  $\eta$  has a larger impact on the mean and median errors in the complex office scene than that in the other two scenes. In addition, mean and median errors increase as the increase of  $\eta$ . As mentioned before, the signal propagation model uses a simple parameter,  $\eta$ , to calibrate the path loss of the entire scene. However, a fixed  $\eta$  cannot represent the variation of a complex scene. In the meantime, the virtual AP based approach leverages the path loss consistency in a small area to estimate the location. The inconsistency between  $\eta$  and virtual AP-based methods in complex environments thus causes a decrease in the localization accuracy. When  $\eta$  is set to 1.6 or smaller, the impact of the parameter on path loss is small. Therefore, the localization error caused by the inconsistency is also reduced. In conclusion, when the proposed method is applied in a simple environment, the optimal value of  $\eta$  is around 1.6. However, a larger  $\eta$  does not make much difference. When the proposed method is applied in a complex environment, the effect of  $\eta$  is greater and the optimal value is below 1.6.

**Table 4.** Impact of different environmental parameters on positioning accuracy in the complex office scene.

	Mean Error (m)	Median Error (m)	70% Error (m)
$\eta = 1.6$	2.71	2.13	3.26
$\eta = 2.0$	2.72	2.15	3.28
$\eta = 2.4$	2.75	2.23	3.29
$\eta = 2.8$	2.76	2.25	3.28
$\eta = 3.2$	2.78	2.27	3.27

## 6. Conclusions

In this paper, we proposed a robust and effective Wi-Fi positioning method. Based on the assumption that neighboring locations share the same attenuation parameter corresponding to the signal attenuation caused by obstacles, we use a virtual AP-based method to improve the accuracy of fingerprinting. By using signal ratios to construct the Apollonius Circle, we reduce the impact of signal attenuation on estimating the virtual location of APs and the online location of MNs. Furthermore, no additional input was introduced, such as the transmission power parameter which is typically required in virtual AP-based methods. The proposed method was compared with three representative Wi-Fi-based positioning approaches in three different test scenes. The results show that the proposed method can achieve state-of-art results in all three scenes. Specifically, it achieves a median distance error of 1.9 m, 2.2 m, and 2.3 m in three test scenes, respectively.

However, there are still some problems that we have not been solved yet: (1) The least square method we use in the virtual AP estimation phase and online positioning phase would easily reach a locally optimal point. (2) The error that happened in the area positioning phase can significantly affect the final location estimation. Solving these problems and investigating how the indoor spatial structure affects the positioning results is our future focus.

**Author Contributions:** Conceptualization, Fan Xu; Data curation, Shuaiwei Luo; Formal analysis, Fan Xu; Methodology, Fan Xu; Resources, Shuaiwei Luo; Software, Fan Xu; Supervision, Jianga Shang; Writing—original draft, Fan Xu; Writing—review and editing, Fan Xu and Xuke Hu. All authors have read and agreed to the published version of the manuscript.

**Funding:** This study was funded by the National Key Research and Development Program of China (No. 2016YFB0502200).

**Conflicts of Interest:** The authors declare no conflict of interest.

## References

1. Chen, R.; Chen, L. Indoor Positioning with Smartphones: The State-of-the-art and the Challenges. *Acta Geod. Cartogr. Sin.* **2017**, *46*, 1316–1326.
2. Shang, J.; Hu, X.; Cheng, W.; Fan, H. GridiLoc: A backtracking grid filter for fusing the grid model with PDR using smartphone sensors. *Sensors* **2016**, *16*, 2137. [[CrossRef](#)]
3. Zhuang, Y.; Lan, H.; Li, Y.; El-Sheimy, N. PDR/INS/WiFi integration based on handheld devices for indoor pedestrian navigation. *Micromachines* **2015**, *6*, 793–812. [[CrossRef](#)]
4. Li, X.; Wang, J.; Liu, C. A Bluetooth/PDR integration algorithm for an indoor positioning system. *Sensors* **2015**, *15*, 24862–24885. [[CrossRef](#)]
5. Ijaz, F.; Yang, H.K.; Ahmad, A.W.; Lee, C. Indoor positioning: A review of indoor ultrasonic positioning systems. In Proceedings of the 2013 15th International Conference on Advanced Communications Technology (ICACT), Phoenix Park, PyeongChang, Korea, 27–30 January 2013; pp. 1146–1150.
6. Priyantha, N.B.; Chakraborty, A.; Balakrishnan, H. The cricket location-support system. In Proceedings of the 6th Annual International Conference on Mobile Computing and Networking, Boston, MA, USA, 6–11 August 2000; pp. 32–43.
7. Luo, J.; Fan, L.; Li, H. Indoor positioning systems based on visible light communication: State of the art. *IEEE Commun. Surv. Tutor.* **2017**, *19*, 2871–2893. [[CrossRef](#)]
8. Wu, T.; Liu, J.; Li, Z.; Liu, K.; Xu, B. Accurate smartphone indoor visual positioning based on a high-precision 3D photorealistic map. *Sensors* **2018**, *18*, 1974. [[CrossRef](#)] [[PubMed](#)]
9. Chapre, Y.; Ignjatovic, A.; Seneviratne, A.; Jha, S. Csi-mimo: Indoor wi-fi fingerprinting system. In Proceedings of the 39th Annual IEEE Conference on Local Computer Networks, Edmonton, AB, Canada, 8–11 September 2014; pp. 202–209.
10. Wang, X.; Gao, L.; Mao, S.; Pandey, S. CSI-based fingerprinting for indoor localization: A deep learning approach. *IEEE Trans. Veh. Technol.* **2016**, *66*, 763–776. [[CrossRef](#)]
11. Li, B.; Gallagher, T.; Dempster, A.G.; Rizos, C. How feasible is the use of magnetic field alone for indoor positioning? In Proceedings of the 2012 International Conference on Indoor Positioning and Indoor Navigation (IPIN), Sydney, Australia, 13–15 November 2012; pp. 1–9.
12. Kim, H.S.; Seo, W.; Baek, K.R. Indoor positioning system using magnetic field map navigation and an encoder system. *Sensors* **2017**, *17*, 651. [[CrossRef](#)]
13. Schmidt, E.; Inupakutika, D.; Mundlamuri, R.; Akopian, D. SDR-Fi: Deep-Learning-Based Indoor Positioning via Software-Defined Radio. *IEEE Access* **2019**, *7*, 145784–145797. [[CrossRef](#)]
14. Chen, L.; Pei, L.; Kuusniemi, H.; Chen, Y.; Kröger, T.; Chen, R. Bayesian fusion for indoor positioning using bluetooth fingerprints. *Wirel. Pers. Commun.* **2013**, *70*, 1735–1745. [[CrossRef](#)]
15. Chen, L.; Kuusniemi, H.; Chen, Y.; Liu, J.; Pei, L.; Ruotsalainen, L.; Chen, R. Constraint Kalman filter for indoor bluetooth localization. In Proceedings of the 2015 23rd European Signal Processing Conference (EUSIPCO), Nice, France, 31 August–4 September 2015; pp. 1915–1919.
16. Zhuang, Y.; Yang, J.; Li, Y.; Qi, L.; El-Sheimy, N. Smartphone-based indoor localization with bluetooth low energy beacons. *Sensors* **2016**, *16*, 596. [[CrossRef](#)] [[PubMed](#)]
17. Wang, H.; Sen, S.; Elgohary, A.; Farid, M.; Youssef, M.; Choudhury, R.R. No need to war-drive: Unsupervised indoor localization. In Proceedings of The 10th International Conference on Mobile Systems, Applications, and Services, Lake District, UK, 26–29 June 2012; pp. 197–210.
18. Shen, G.; Chen, Z.; Zhang, P.; Moscibroda, T.; Zhang, Y. Walkie-Markie: Indoor pathway mapping made easy. In Proceedings of the 10th {USENIX} Symposium on Networked Systems Design and Implementation ({NSDI} 13), Lombard, IL, USA, 2–5 April 2013; pp. 85–98.

19. Kim, Y.; Shin, H.; Cha, H. Smartphone-based Wi-Fi pedestrian-tracking system tolerating the RSS variance problem. In Proceedings of the 2012 IEEE International Conference on Pervasive Computing and Communications, Lugano, Switzerland, 19–23 March 2012; pp. 11–19.
20. Palumbo, F.; Barsocchi, P.; Chessa, S.; Augusto, J.C. A stigmergic approach to indoor localization using bluetooth low energy beacons. In Proceedings of the 2015 12th IEEE International Conference on Advanced Video and Signal Based Surveillance (AVSS), Karlsruhe, Germany, 25–28 August 2015; pp. 1–6.
21. Zhao, X.; Xiao, Z.; Markham, A.; Trigoni, N.; Ren, Y. Does BTLE measure up against WiFi? A comparison of indoor location performance. In Proceedings of the European Wireless 2014, 20th European Wireless Conference, Castelldefels, Spain, 14–16 May 2014; pp. 1–6.
22. Rusli, M.E.; Ali, M.; Jamil, N.; Din, M.M. An improved indoor positioning algorithm based on rssi-trilateration technique for internet of things (iot). In Proceedings of the 2016 International Conference on Computer and Communication Engineering (ICCCCE), Kuala Lumpur, Malaysia, 25–27 July 2016; pp. 72–77.
23. Dag, T.; Arsan, T. Received signal strength based least squares lateration algorithm for indoor localization. *Comput. Electr. Eng.* **2018**, *66*, 114–126. [[CrossRef](#)]
24. Jung, J.; Myung, H. Range-based indoor user localization using reflected signal path model. In Proceedings of the 5th IEEE International Conference on Digital Ecosystems and Technologies (IEEE DEST 2011), Daejeon, Korea, 31 May–3 June 2011; pp. 251–256.
25. Chuang, P.J.; Wu, C.P. Employing PSO to enhance RSS range-based node localization for wireless sensor networks. *J. Inf. Sci. Eng.* **2011**, *27*, 1597–1611.
26. Chan, F.K.; So, H.C. Accurate distributed range-based positioning algorithm for wireless sensor networks. *IEEE Trans. Signal Process.* **2009**, *57*, 4100–4105. [[CrossRef](#)]
27. Coluccia, A.; Ricciato, F. RSS-based localization via Bayesian ranging and iterative least squares positioning. *IEEE Commun. Lett.* **2014**, *18*, 873–876. [[CrossRef](#)]
28. Liu, C.; Scott, T.; Wu, K.; Hoffman, D. Range-free sensor localisation with ring overlapping based on comparison of received signal strength indicator. *IJSSNet* **2007**, *2*, 399–413. [[CrossRef](#)]
29. Rajagopal, N.; Chayapathy, S.; Sinopoli, B.; Rowe, A. Beacon placement for range-based indoor localization. In Proceedings of the 2016 International Conference on Indoor Positioning and Indoor Navigation (IPIN), Sapporo, Japan, 18–21 September 2016; pp. 1–8.
30. Elbakly, R.; Youssef, M. A robust zero-calibration RF-based localization system for realistic environments. In Proceedings of the 2016 13th Annual IEEE International Conference on Sensing, Communication, and Networking (SECON), London, UK, 27–30 June 2016; pp. 1–9.
31. Lasla, N.; Younis, M.F.; Ouadjaout, A.; Badache, N. An effective area-based localization algorithm for wireless networks. *IEEE Trans. Comput.* **2014**, *64*, 2103–2118. [[CrossRef](#)]
32. He, T.; Huang, C.; Blum, B.M.; Stankovic, J.A.; Abdelzaher, T. Range-free localization schemes for large scale sensor networks. In Proceedings of the 9th Annual International Conference on Mobile Computing and Networking, San Diego, CA, USA, 14–19 September 2003; pp. 81–95.
33. Sheu, J.P.; Chen, P.C.; Hsu, C.S. A distributed localization scheme for wireless sensor networks with improved grid-scan and vector-based refinement. *IEEE Trans. Mob. Comput.* **2008**, *7*, 1110–1123. [[CrossRef](#)]
34. Dai, H.; Ying, W.H.; Xu, J. Multi-layer neural network for received signal strength-based indoor localisation. *IET Commun.* **2016**, *10*, 717–723. [[CrossRef](#)]
35. Khatab, Z.E.; Hajihoseini, A.; Ghorashi, S.A. A fingerprint method for indoor localization using autoencoder based deep extreme learning machine. *IEEE Sens. Lett.* **2017**, *2*, 1–4. [[CrossRef](#)]
36. Li, Z.; Xu, K.; Wang, H.; Zhao, Y.; Wang, X.; Shen, M. Machine-Learning-Based Positioning: A Survey and Future Directions. *IEEE Netw.* **2019**, *33*, 96–101. [[CrossRef](#)]
37. Salamah, A.H.; Tamazin, M.; Sharkas, M.A.; Khedr, M. An enhanced WiFi indoor localization system based on machine learning. In Proceedings of the 2016 International Conference on Indoor Positioning and Indoor Navigation (IPIN), Alcalá de Henares, Madrid, Spain, 4–7 October 2016; pp. 1–8.
38. Nerguizian, C.; Nerguizian, V. Indoor fingerprinting geolocation using wavelet-based features extracted from the channel impulse response in conjunction with an artificial neural network. In Proceedings of the 2007 IEEE International Symposium on Industrial Electronics, Vigo, Spain, 4–7 June 2007; pp. 2028–2032.
39. Shang, J.; Hu, X.; Gu, F.; Wang, D.; Yu, S. Improvement schemes for indoor mobile location estimation: A survey. *Math. Probl. Eng.* **2015**, *2015*. [[CrossRef](#)]

40. Xue, W.; Yu, K.; Hua, X.; Li, Q.; Qiu, W.; Zhou, B. APs's virtual positions-based reference point clustering and physical distance-based weighting for indoor Wi-Fi positioning. *IEEE Internet Things J.* **2018**, *5*, 3031–3042. [[CrossRef](#)]
41. Mo, Y.; Cai, Y.; Wang, B. A novel indoor localization method based on virtual AP estimation. In Proceedings of the 2012 IEEE International Conference on Communications (ICC), Ottawa, ON, Canada, 10–15 June 2012; pp. 5508–5512.
42. Liu, H.H.; Yang, Y.N. Wi-Fi-based indoor positioning for multi-floor environment. In Proceedings of the TENCON 2011-2011 IEEE Region 10 Conference, Bali, Indonesia, 21–24 November 2011; pp. 597–601.
43. Coolidge, J.L. *A Treatise on the Circle and the Sphere*; Clarendon Press: Oxford, UK, 1916.
44. He, S.; Chan, S.H.G. Wi-Fi fingerprint-based indoor positioning: Recent advances and comparisons. *IEEE Commun. Surv. Tutor.* **2015**, *18*, 466–490. [[CrossRef](#)]
45. Feng, C.; Au, W.S.A.; Valaee, S.; Tan, Z. Received-signal-strength-based indoor positioning using compressive sensing. *IEEE Trans. Mob. Comput.* **2011**, *11*, 1983–1993. [[CrossRef](#)]
46. Au, A.W.S.; Feng, C.; Valaee, S.; Reyes, S.; Sorour, S.; Markowitz, S.N.; Gold, D.; Gordon, K.; Eizenman, M. Indoor tracking and navigation using received signal strength and compressive sensing on a mobile device. *IEEE Trans. Mob. Comput.* **2012**, *12*, 2050–2062. [[CrossRef](#)]
47. He, S.; Chan, S.H.G. Tilejunction: Mitigating signal noise for fingerprint-based indoor localization. *IEEE Trans. Mob. Comput.* **2015**, *15*, 1554–1568. [[CrossRef](#)]
48. He, S.; Chan, S.H.G. Sectjunction: Wi-Fi indoor localization based on junction of signal sectors. In Proceedings of the 2014 IEEE International Conference on Communications (ICC), Sydney, Australia, 10–14 June 2014; pp. 2605–2610.
49. Jiang, Y.; Pan, X.; Li, K.; Lv, Q.; Dick, R.P.; Hannigan, M.; Shang, L. Ariel: Automatic wi-fi based room fingerprinting for indoor localization. In Proceedings of the 2012 ACM conference on ubiquitous computing, Pittsburgh, PA, USA, 5–8 September 2012; pp. 441–450.
50. Shin, B.; Lee, J.H.; Lee, T.; Kim, H.S. Enhanced weighted K-nearest neighbor algorithm for indoor Wi-Fi positioning systems. In Proceedings of the 2012 8th International Conference on Computing Technology and Information Management (NCM and ICNIT), Seoul, Korea, 24–26 April 2012; Volume 2, pp. 574–577.
51. Yang, Z.; Wu, C.; Liu, Y. Locating in fingerprint space: wireless indoor localization with little human intervention. In Proceedings of the 18th Annual International Conference on Mobile Computing and Networking, Istanbul, Turkey, 22–26 August 2012; pp. 269–280.
52. Liu, S.; Hua, X.; Qiu, W.; Zhang, W.; He, X. An improved WiFi fingerprint positioning algorithm. *J. Geomat.* **2017**, *42*, 46–49.
53. Niu, J.; Wang, B.; Shu, L.; Duong, T.Q.; Chen, Y. ZIL: An energy-efficient indoor localization system using ZigBee radio to detect WiFi fingerprints. *IEEE J. Sel. Areas Commun.* **2015**, *33*, 1431–1442. [[CrossRef](#)]
54. Hu, X.; Shang, J.; Gu, F.; Han, Q. Improving Wi-Fi indoor positioning via AP sets similarity and semi-supervised affinity propagation clustering. *Int. J. Distrib. Sens. Netw.* **2015**, *11*, 109642. [[CrossRef](#)]
55. Labinghisa, B.; Park, G.S.; Lee, D.M. Improved indoor localization system based on virtual access points in a Wi-Fi environment by filtering schemes. In Proceedings of the 2017 International Conference on Indoor Positioning and Indoor Navigation (IPIN), Sapporo, Japan, 18–21 September 2017; pp. 1–7.
56. Lee, D.M.; Labinghisa, B. Indoor localization system based on virtual access points with filtering schemes. *Int. J. Distrib. Sens. Netw.* **2019**, *15*, 1550147719866135. [[CrossRef](#)]
57. Xue, W.; Qiu, W.; Hua, X.; Yu, K. Improved Wi-Fi RSSI measurement for indoor localization. *IEEE Sens. J.* **2017**, *17*, 2224–2230. [[CrossRef](#)]
58. Bahl, P.; Padmanabhan, V.N. RADAR: An in-building RF-based user location and tracking system. In Proceedings of the IEEE INFOCOM 2000 Conference on Computer Communications. Nineteenth Annual Joint Conference of the IEEE Computer and Communications Societies (Cat. No. 00CH37064), el Aviv, Israel, 26–30 March 2000; Volume 2, pp. 775–784.
59. Chen, J.; Wang, S.; Ouyang, M.; Xuan, Y.; Li, K.C. Iterative Positioning Algorithm for Indoor Node Based on Distance Correction in WSNs. *Sensors* **2019**, *19*, 4871. [[CrossRef](#)] [[PubMed](#)]

